Time-dependent fracture of cementitious materials

G.P.A.G. van Zijl
Faculty of Architecture, Delft University of Technology, Berlageweg 1, 2628 CR Delft, The Netherlands

René de Borst
Koiter Institute/Faculty of Aerospace Engineering, Delft University of Technology, Kluyverweg 1, 2629 HS Delft, The Netherlands

Jan G. Rots
Faculty of Architecture, Delft University of Technology, Berlageweg 1, 2628 CR Delft, The Netherlands

The response of cementitious materials is highly time dependent. On the one hand, it can lead to delayed collapse of structures fabricated of such materials. On the other hand, the time dependence is associated with the relaxation of peak stresses, which avoids, or postpones damage. A finite element formulation is presented for the analysis of the time-dependent cracking of cementitious materials. The constitutive law incorporates continuum plasticity and linear visco-elasticity. The former accounts for crack initiation and propagation, while the latter describes the bulk creep via an aging Maxwell chain. The cracking velocity dependence, which considers the additional viscous effect in the fracture process zone, is also included. This contribution to the cracking resistance regularises the localisation process and also introduces the correct time scale. The simple framework of the model allows the inclusion of other important phenomena in cementitious materials, such as stress-dependent hygral and thermal shrinkage.

Key words: **Concrete, fracture, creep, shrinkage, crack rate**

1 Introduction

Intense research efforts have gone into the description of fracture in cementitious materials during the last few decades. Insight has been gained in the fracture processes via experiments. With this knowledge, mathematical models have been formulated, for which numerical solutions have been derived. All this has been done in strife of a prediction capability of the material behaviour under mechanical and environmental loads, to facilitate the integrity in terms of safety and serviceability of structures fabricated of these materials.
However, much less attention has been given to the time dependence of the fracture processes in these materials. A crack opens at a finite rate, which fact may be either detrimental or beneficial to

structural integrity and serviceability. Due to time-dependent crack growth and the degradation of the material by the creep mechanisms, a concrete or masonry structure may collapse after some time under a sustained/creep load. Depending on the creep load level, the failure may be delayed for a few seconds, or for many years, for example the collapse of the civic tower of Pavia after nine centuries (Binda et al. 1992). On the other hand, creep/relaxation relaxes the peak stresses caused by internal or external restraint to slow thermal and hygral shrinkage evolutions. Thereby, cracking is avoided or postponed. It is imperative that the time-dependent behaviour is understood and predictable to avoid unexpected failure or loss of serviceability, but also to exploit the "forgiving" nature of the material to low rate processes.

This papers presents a numerical (finite element) model, which considers the most important phenomena governing the time-dependent response of masonry. Two sources of time dependence are considered, namely the bulk/volumous creep and the rate dependence in the fracture process zone (FPZ). The former is modelled with linear visco-elasticity, justified by the linearity of the tensile creep isochrones of concrete. For the rate source in the FPZ two models are considered, namely a three-parameter model derived from the rate process theory and a single-parameter crack viscosity model. The cracking is captured either in a smeared, continuous way, or in a discrete strategy, which requires pre-knowledge where cracks may occur, for example the joints in masonry. In both cases constitutive laws based in computational plasticity are employed (Lourenço 1996, van Zijl 2000). The model is validated by the analysis of creep failure experiments performed by Zhou (1992) on concrete beams in three-point bending.

Subsequently, the environmental actions which have a large influence on concrete and masonry, namely hygral and thermal shrinkage, are addressed. Both these sources of dimensional change are incorporated in the numerical model, but have to be determined before the mechanical analysis. A nonlinear diffusion formulation for the description of the pore relative humidity evolution in cementitious materials, which is the driving force behind hygral shrinkage, is elaborated. The heat conduction, which drives the thermal shrinkage, is analogous to the pore humidity diffusion process, but is not discussed. To demonstrate this one-way coupled analysis of shrinkage evolution and the mechanical response to it, masonry creep and shrinkage experiments (van der Pluijm and Wubs 1996) are analysed.

2 A rate-type constitutive law

Due to the nonlinearity of the time-dependent behaviour of cementitious materials, a rate form is adopted for the constitutive relation. It is assumed that the strain rate can be decomposed as follows:

$$\dot{\varepsilon} = \dot{\varepsilon}_{ve} + \dot{\varepsilon}_{cr} + \dot{\varepsilon}_{s} + \dot{\varepsilon}_{T}. \qquad (1)$$

where ε_{ve} is the vector of visco-elastic strains, ε_{cr} is the vector of cracking strains and ε_{s} and ε_{T} are the vectors of hygral and thermal shrinkage respectively.

The linear-viscoelastic constitutive law can be expressed in the following rate form (de Borst 1986, van Zijl 2000)

$$\dot{\sigma} = \boldsymbol{D}^{ve}\dot{\varepsilon}_{ve} + \Sigma, \tag{2}$$

where $\boldsymbol{D}^{ve}$ is an equivalent, time-dependent stiffness modulus, $\dot{\varepsilon}_{ve}$ is the visco-elastic strain rate and Σ is a viscous stress term which accounts for the history. The combination of eqs. (1) and (2) produces the stress rate

$$\dot{\sigma} = \boldsymbol{D}^{ve}(\dot{\varepsilon} - \dot{\varepsilon}_{cr} - \dot{\varepsilon}_{s} - \dot{\varepsilon}_{T}) + \Sigma. \tag{3}$$

Upon integration, eq. (3) becomes

$$\Delta\sigma = \boldsymbol{D}^{ve}(\Delta\varepsilon - \Delta\varepsilon_{cr} - \Delta\varepsilon_{s} - \Delta\varepsilon_{T}) + {}^{t}\tilde{\sigma}, \tag{4}$$

where

$$\begin{aligned} \boldsymbol{D}^{ve} &= \left[E_0(t^*) + \sum_{n=1}^{N}\left(1 - e^{-\frac{\Delta t}{\zeta_n}}\right)\frac{E_n(t^*)}{\Delta t/\zeta_n}\right]D \\ {}^{t}\tilde{\sigma} &= -\sum_{n=1}^{N}\left(1 - e^{-\frac{\Delta t}{\zeta_n}}\right){}^{t}\sigma_n. \end{aligned} \tag{5}$$

2.1 *The creep formulation*

In eqs. (4,5) an aging Maxwell chain can be identified, with time dependent element stiffnesses $E_n(t)$ and viscosities $\eta_n = E_n\zeta_n$, where ζ_n is the relaxation time of dashpot n, $n = 1,2,...,N$. The parameters are assumed to be constant in each time interval. They are evaluated at a time $t \le t^* \le t + \Delta t$. The stress vector ${}^{t}\sigma_n$ contains the stress components in chain element n at the end of the previous time step, i.e. at time t. $\boldsymbol{D}$ is a dimensionless matrix which is dependent on Poisson's ratio ν (de Borst et al. 1993, van Zijl 2000). In Figure 1 the creep model is schematised.

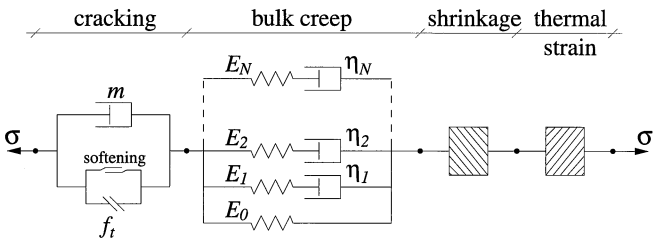

Fig. 1. Maxwell chain model with cracking, thermal and shrinkage strain elements in series.

2.2 *Cracking*

Computational plasticity is a convenient framework for the modelling of cracking in cementitious materials (e.g. Feenstra 1993, Lourenço 1996, van Zijl 2000). Thereby, the crack strain increment in eq. (4), also schematised in Figure 1, follows from the plastic flow

$$\Delta\varepsilon_{cr} = \Delta\kappa\frac{\partial g}{\partial\sigma}, \tag{6}$$

with $g(\sigma, \kappa)$ the plastic potential function, of which the stress gradient defines the cracking direction and $\Delta\kappa$ the amount of cracking strain. The stress is limited by the yield function/limit surface

$$f(\sigma, \kappa) \leq 0. \tag{7}$$

The particular choice of limit surface depends on the modelling strategy. In masonry, it makes sense to model the cracking in a discrete strategy, because the joints are known to be the weak links where cracking will occur. In a detailed discrete approach both the bricks and mortar are discretised, while interface elements between these two constituents account for the cracking. This can be simplified by lumping the total joint behaviour into interface elements. Then, only the bricks are discretised with continuum elements. In both cases, potential vertical cracks may also be provided for through the centre of the bricks, by placing interface elements there. This extension enables the reasonably accurate analysis of masonry with relatively weak bricks. When the location and orientation of cracks are known, concrete cracking may also be modelled with the discrete strategy.
The interface elements obey an interface material law, which combines a Coulomb friction criterion and a tensile cut-off, Figure 2. The limit surfaces, softening descriptions and computational details are given in van Zijl (2000).

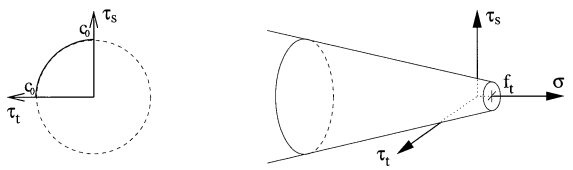

Fig. 2. Interface material model for discrete modelling strategy.

Alternatively, the cracking is modelled in a smeared way in a continuum plasticity formulation. This approach is appropriate for concrete, where the aggregate size is small relative to the structural dimension and it is not known before where cracks will occur. It may also be applied to masonry with a large structural dimension/brick size ratio. In this case the heterogeneity is ignored and continuum elements span across phase boundaries. An anisotropic Rankine limit surface is appropriate for masonry (Lourenço 1996), while the isotropic option for concrete can be activated by the correct parameter choice. In plane stress this limit surface reads

$$f = \frac{(\sigma_x - \sigma_{tx}) + (\sigma_y - \sigma_{ty})}{2} + \sqrt{\left(\frac{(\sigma_x - \sigma_{tx}) + (\sigma_y - \sigma_{ty})}{2}\right)^2 + \alpha\tau^2_{xy}}, \tag{8}$$

which is shown schematically in Figure 3. The coefficient α controls the shear stress contribution to failure. With $\alpha = 1$, eq. (8) is a maximum principal stress limit surface.
The potential function has been chosen as

$$g = f|_{\alpha = 1}. \tag{9}$$

The softening in the orthogonal directions is described by the exponential degradation of the cracking stresses

$$\sigma_{tx} = f_{tx} e^{-\frac{f_{tx}}{g_{fx}}\kappa} \quad , \quad \sigma_{ty} = f_{ty} e^{-\frac{f_{ty}}{g_{fy}}\kappa} \tag{10}$$

with f_{tx} and f_{ty} the tensile strengths and g_{fx} and g_{fy} the fracture energies in the orthogonal directions.

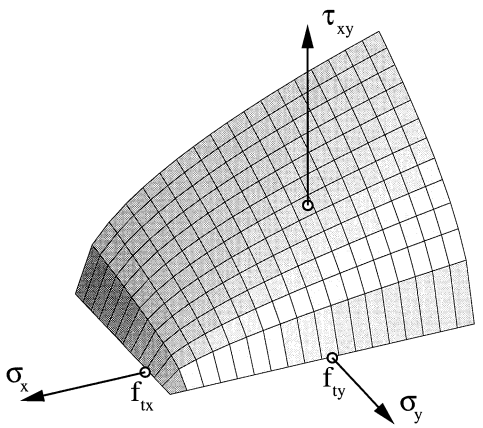

Fig. 3. Anisotropic Rankine model for continuous/smeared crack modelling (Lourenço 1996).

2.3 *The FPZ viscosity*

The cracking stress formulations (10) are independent of the cracking velocity. To consider the viscosity in the FPZ, eq. (10) is supplemented with rate terms. Two alternative formulations are employed. A three-parameter model derived from the rate process theory by Wu and Bazant (1993) modifies the cracking stress to read

$$\begin{aligned} \sigma_{tx} &= f_{tx} e^{-\frac{f_{tx}}{g_{fx}}\kappa} \left[1 + k_0 \sinh^{-1}\left(\frac{\dot{\kappa}}{\dot{\kappa}_r}\right)\right] + k_0 k_1 f_{tx} \sinh^{-1}\left(\frac{\dot{\kappa}}{\dot{\kappa}_r}\right) \\ \sigma_{ty} &= f_{ty} e^{-\frac{f_{ty}}{g_{fy}}\kappa} \left[1 + k_0 \sinh^{-1}\left(\frac{\dot{\kappa}}{\dot{\kappa}_r}\right)\right] + k_0 k_1 f_{ty} \sinh^{-1}\left(\frac{\dot{\kappa}}{\dot{\kappa}_r}\right). \end{aligned} \tag{11}$$

The model parameter k_0 is estimated to be in the range 0.01 - 0.08 from the knowledge that for a 10^4-fold increase of the loading rate a 25% increase in peak strength is found experimentally. The model parameter k_1 is an offset factor which accounts for the long tail in the load-deformation response of cementitious materials. $\dot{\kappa}_r$ is a low, constant reference crack opening strain rate.
A simple alternative is to assume that the crack opening viscosity is m, Figure 1, which leads to the formulation

$$\sigma_{tx} = (f_{tx} + m\dot{\kappa}) e^{-\frac{f_{tx}}{g_{fx}}\kappa} , \qquad \sigma_{tx} = (f_{ty} + m\dot{\kappa}) e^{-\frac{f_{ty}}{g_{fy}}\kappa} . \tag{12}$$

2.4 *Discussion of mechanical model*

It should be noted that in the discrete crack modelling approach, the cracking is captured in the interfaces, while the creep and shrinkage are captured by the continuum elements. In the continuum approach, all these components are active in the continuum, as schematised in Figure 1 and implicated by eq. (4).

It has been shown that the FPZ rate dependence regularises the continuum description of localisation (Sluys 1992, de Borst et al. 1993, van Zijl 2000). The numerical difficulties and mesh-dependent results obtained with standard continuum cracking models do not occur. However, in the next section it is shown that the rate terms are not included merely for numerical reasons, but that they fulfill the physical role of introducing the correct time scale and correctly account for the strength increase with increased loading rate.

The nonlinear governing equations are solved in an incremental-iterative way, as described by van Zijl (2000). A consistent tangent modulus has been formulated, which leads to quadratic convergence of the global solution.

3 Validation: Creep failure tests

To validate that the model can capture the intricate interaction between the viscous processes in cementitious materials, the three-point bending creep tests performed by Zhou (1992) on concrete beams are analysed. The concrete specimens were kept at hygral and thermal equilibrium to avoid the further complication introduced by the simultaneous drying and thermal shrinkage.

3.1 *Description of the tests*

The geometry and set-up of the 100 *mm* thick notched concrete beams which were tested by Zhou, is schematised in Figure 4a. Zhou performed displacement-controlled tests to obtain the total load-deformation response. In subsequent tests he employed force control to study the time-dependent interaction of creep and cracking. In these tests the central force was increased gradually to a predefined level, which was subsequently sustained. A sustained load of larger than about 60% of the peak load eventually led to failure of the beams. Two displacement-controlled tests were performed at 5 $\mu m/s$. The responses are shown in Figure 4b. Also shown are the average results of the sustained load tests, 2 at 92%, 2 at 85%, 4 at 80% and 3 at 76% of the average peak load of the displacement-controlled cases. The average crack mouth opening displacement (CMOD) at failure under each sustained load is indicated by a dot, while the ranges are indicated by vertical lines.

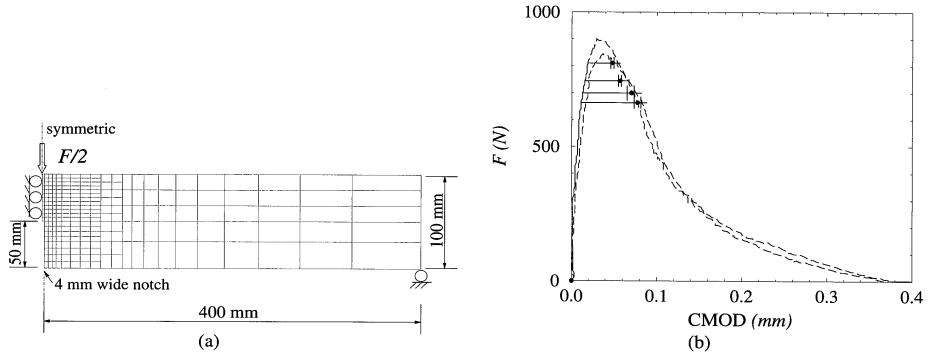

Fig. 4. Three-point bending tests. (a) Specimen geometry, set-up and FE model, (b) CMOD measurements (Zhou 1992), indicating range in failure values.

3.2 *Finite element model*

The finite element mesh employed for the analyses is also shown in Figure 4a. It consists of plane-stress, four-noded quadrilateral elements. Symmetry is exploited, enabling one half of the model only to be modelled.

To study the cracking rate dependence, the formulation proposed by Wu and Bazant (1993), eq. (11), as well as the simple cracking viscosity model, eq. (12), are employed. Bulk creep is considered by activating the Maxwell chain incorporated in the constitutive model. The own weight is compensated for by applying a volume load of mass density 2400 kg/m^3 in an initial step in each analysis. Separate tests had been performed to determine the material parameters, yielding a Young's modulus 36 *GPa* and the tensile strength f_t = 2.8 *MPa* (Zhou 1992). Also, relaxation tests had been performed on cylindrical, notched tensile specimens, providing information for determining the bulk creep parameters, Figure 5. A 10-element Maxwell chain model has been fitted by a least squares method to the relaxation curve - Figure 5. Unfortunately, the relaxation was measured over short times (maximum 1 hour), calling for extrapolation. An extremely high creep coefficient $\phi = \varepsilon_c/\varepsilon_e = 5$ has been assumed after 100 days. This has been done to numerically maximise the role of the bulk creep in the creep fracture process and thereby to demonstrate that, despite such a large rate contribution by the bulk creep, the crack rate dependence must be added to simulate the measured responses.

Zhou (1992) has also performed three-point bending tests under displacement control on smaller beams (600 *mm* long by 50 × 50 mm^2 section) to determine the fracture energy G_f. By varying the deflection rate from slow (0.05 μ *m/s* - peak load after about 80 minutes) to fast (50 μ *m/s* - peak load after about 5 *s)* he studied the rate influence on the fracture energy, Figure 6a, and peak strength, Figure 6 b. To derive the parameters for the FPZ rate models, eqs. (11,12), a process of inverse fitting has been followed. For these analyses the smaller beam has been modelled with the same mesh shown in Figure 4a, scaled to the small beam geometry. The parameters which have been obtained in this way are, for eq. (11): $k_0 = 0.05$, $k_1 = 0.1$, $\dot{K}_r = 10^{-7} s^{-1}$ and for eq. (12): $m = 1500\ Ns/mm^2$. In figure 6b the normalised numerical peak strengths are compared with the measured values. Reasonable

agreement is found with the three-parameter model, but with the simple one-parameter model it is impossible to fit the strength increase over the entire range of loading rates. A possible remedy is to employ a rate-dependent viscosity m ($\dot{\kappa}$). This has not been attempted. Instead, the three-parameter model has been employed for the subsequent analyses.

With regard to the apparent increase in fracture energy with loading rate, it must be noted that this follows from the numerical model although constant fracture energy is prescribed. This value can be estimated by extrapolation to the deflection rate at the reference CMO strain rate $\dot{\kappa}$, Figure 6a. A constant value of $G_f = 0.035$ *N/mm* has been used.

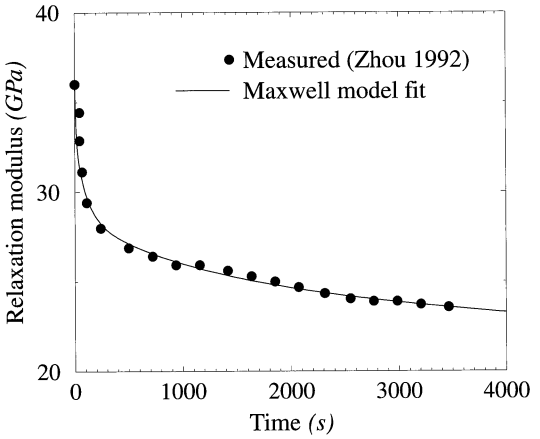

Fig. 5. Maxwell chain fit to the relaxation data.

3.3 *Results*

The displacement-controlled cases are analysed first, with the deflection rate 5 $\mu m/s$, as employed in the experiment. Figure 7a compares the numerical response with the experimental responses.

To obtain this agreement a 5% lower tensile strength than the reported f_t =2.8 *MPa* (Zhou 1992) and a Young's modulus 30 *GPa* have been used. On the one hand these adjustments have been made to give reasonable agreement with the experimental responses, in order to make possible the subsequent comparison between the responses under sustained load. On the other hand the strength and stiffness are rate dependent. Thus, the reduction of the measured parameters is in line with the determination of the "rate-independent" values, as has been done in the previous section for the fracture energy.

Next, the sustained load cases are analysed, Figure 7b. As was attempted in the experiments (Zhou 1992), the initial, ascending loading rate is the same as for the displacement-controlled case. Beyond this ascending branch the load level is kept constant and the creep behaviour is analysed. During this stage the crack propagates and the deflection and CMOD increase up to a point where equilibrium can no longer be achieved for the sustained load level. Here, the load bearing capacity of the beam is exceeded. To ensure that failure under the sustained load is indeed imminent, the analyses are continued, by replacing the force control with displacement control at this point. This results in the subsequent softening responses which prove that failure would have occurred under continued

load control. These results confirm the experimental observation that the displacement-controlled response serves as an envelope for failure under sustained loads.

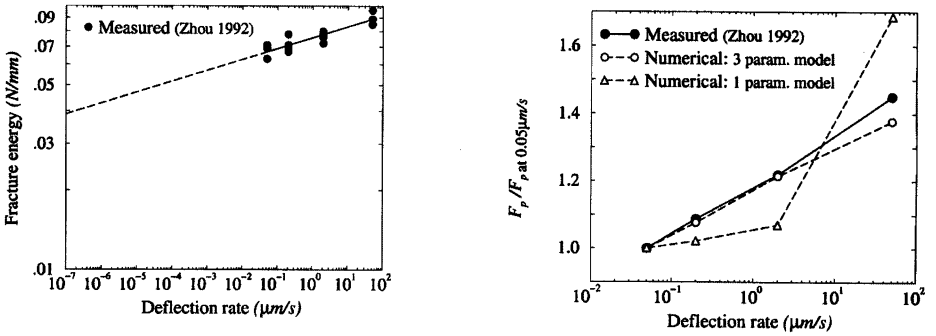

(a) (b)

Fig. 6. Rate effect on (a) fracture energy and (b) peak strength (Zhou 1992).

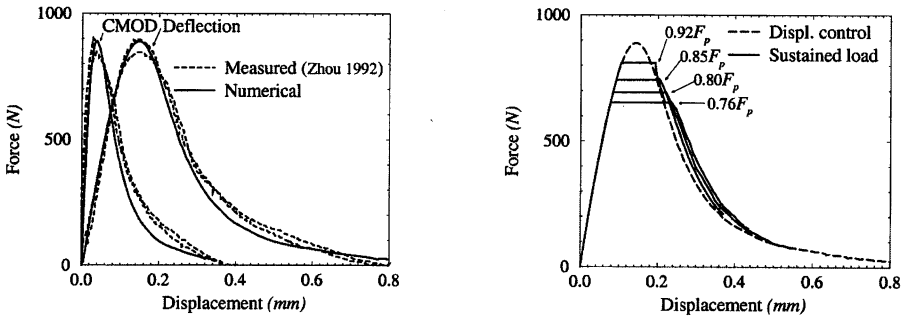

(a) (b)

Fig. 7. (a) Comparison of experimental and numerical displacement-controlled (5 μm/s) responses. (b) Numerical creep responses, with switch to displacement control at failure.

The CMODs computed numerically compare reasonably with the measured values, Figure 8a. If the crack rate dependence is ignored, this is not the case. Furthermore, apart from simulating the deformational response, it is imperative that the time scale involved is captured accurately by the model. Reasonable agreement is found with the measured times between reaching the sustained load level and failure, Figure 8b. However, if the crack rate dependence is not activated, these times are greatly overestimated. This provides strong evidence of the validity of the inclusion of the cracking rate dependence.

F/F_p	0.92	0.85	0.80	0.76
Measured CMOD (μm): (average, Zhou 1992)	48	57	70	77
Numerical (μm):	56	59	67	72
Numerical (μm): (Bulk creep only)	52	73	88	102

(a)

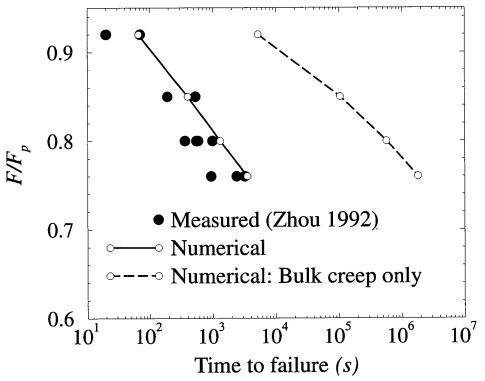

(b)

Fig. 8. Three-point bending (a) CMOD at the point of failure and (b) time to failure under sustained load.

4 Hygral and thermal shrinkage

The mechanical model (3) provides for the inclusion of thermal and hygral shrinkage. In a macroscopic approach they can be considered to be driven by diffusive processes of heat conduction and moisture migration respectively. In the absence of large cracks these processes are uni-laterally coupled with the mechanical process. For instance, unlike a sponge, water is not squeezed out of concrete by compression (L'Hermite and Mamillan 1968). This means the shrinkage evolutions can be calculated independent of the mechanical stresses in an initial step and subsequently included in the mechanical analysis. In this section a finite element formulation for the computation of the hygral shrinkage evolution is presented. The thermal shrinkage formulation is analogous. Note, however, that a fully coupled set of differential equations have to be solved for simultaneous hygral and thermal variation. This is not considered here.

4.1 *Moisture migration in cementitious materials*

The moisture flow in a non-saturated, porous medium under hygral and thermal gradients can be described by the nonlinear diffusion-type equation

$$\begin{aligned} &\frac{d\theta}{dt} + \nabla \cdot \boldsymbol{q} + Q = 0 \\ &\boldsymbol{q} = -\boldsymbol{d}_\theta \nabla\theta - \boldsymbol{d}_T \nabla T \end{aligned} \tag{13}$$

where θ is the total moisture content in liquid and vapour phases and Q is the rate of moisture loss due to hydration (Philip and De Vries 1957, Pel 1995). The moisture diffusivity $\boldsymbol{d}_\theta$ as well as the thermal moisture diffusivity $\boldsymbol{d}_T$ are strongly dependent on the moisture content, which causes the nonlinearity of eq. (13). For convenience, the diffusion process is written in terms of the relative pore humidity

$$h = p/p_s, \tag{14}$$

with p the macroscopical pore pressure and p_s the macroscopical pore pressure at saturation. Since $\theta = \theta(p, T)$ and thus $\theta = \theta(h, T)$ eq. (13) becomes

$$\begin{aligned} \frac{dh}{dt} &= -c^{-1}(\nabla \cdot \boldsymbol{q} + Q) - \frac{\partial h}{\partial T}\frac{\partial T}{\partial t} \\ \boldsymbol{q} &= -\boldsymbol{d}_h \nabla h - \left(\boldsymbol{d}_T + \boldsymbol{d}_\theta \frac{\partial \theta}{\partial T}\right)\nabla T, \end{aligned} \tag{15}$$

where

$$\begin{aligned} c &= \frac{\partial \theta}{\partial h} \\ \boldsymbol{d}_h &= \boldsymbol{d}_\theta c. \end{aligned} \tag{16}$$

The parameters in eq. (15) can be interpreted physically. The gradient of the hygroscopic relation c reflects the ability to absorb or release water under unit change in h. Furthermore, $\boldsymbol{d}_h$ has been shown to represent permeability (Bažant and Najjar 1971). An added benefit of this formulation is that the influence of the continued hydration can usually be ignored (Bažant 1988). For isothermal conditions eq. (15) reduces to

$$\begin{aligned} \dot{h} &= -c^{-1}\nabla \cdot \boldsymbol{q} \\ \boldsymbol{q} &= \boldsymbol{d}_h \nabla h. \end{aligned} \tag{17}$$

4.1.1 Boundary and initial conditions

A further advantage of employing the relative pore humidity as potential for the diffusion equation is that the boundary conditions can be easily identified:

essential,	i.e. prescribed humidity:	$h_B = h_E$	
natural,	i.e. prescribed boundary flux:	$\boldsymbol{q} \cdot \boldsymbol{n} = -q_B$	(18)
convective:		$\boldsymbol{q} \cdot \boldsymbol{n} = \beta(h - h_E)$	

with $\boldsymbol{n}$ the unit vector pointing outward and normal to the boundary, the subscript B denoting the boundary and the subscript E denoting the prescribed, or environmental value. The surface convection coefficient β, also referred to as the film coefficient, is given by

$$\beta = \frac{\beta^* p_s}{\rho_l} \tag{19}$$

with β^* (s/m) the transfer coefficient depending mainly on air velocity and surface smoothness (Tammes and Vos 1984) and ρ_l (kg/m^3) the liquid moisture mass density.

4.1.2 Solution of the governing diffusion equation

For the numerical (finite element) solution of the governing differential equation (17), it is subjected to the Galerkin method of weighted residuals. This is a well-established procedure and described in detail by, for instance, Becker et al. (1981). For the full details of the numerical solution procedure followed in this study, the reader is referred to van Zijl (2000).

4.2 *From pore humidity/temperature to shrinkage*

The drying shrinkage of cementitious materials is driven by the pore pressure (Wittmann 1977, Bažant 1988). It is usually obtained from the incremental relation:

$$\dot{\varepsilon}_{s,o} = \alpha_s \dot{h}. \tag{20}$$

Experimental measurements indicate that the shrinkage coefficient α_s is approximately constant in the range $0.4 \leq h \leq 0.99$, but a polynomial function of h may be more appropriate (van Zijl 1999). This poses no mathematical or numerical difficulty, but until more experimental evidence is obtained, the constant relation is assumed. Eq. (20) can be generalised to three dimensions and orthotropy:

$$\dot{\boldsymbol{\varepsilon}}_s = \dot{\varepsilon}_{s,o} \boldsymbol{P}_s, \tag{21}$$

where $\boldsymbol{P}_s$ is a scaling, normalised vector defined as

$$\boldsymbol{P}_s = [P_{sx} P_{sy} P_{sz} 0\ 0\ 0]^T. \tag{22}$$

The thermal strains are related to the temperature in a similar way:

$$\dot{\boldsymbol{\varepsilon}}_T = \dot{\varepsilon}_{T,o} \boldsymbol{P}_T, \tag{23}$$

with

$$\dot{\varepsilon}_{T,o} = \alpha_T \dot{T}, \tag{24}$$

where α_T is the thermal expansion coefficient and

$$\boldsymbol{P}_T = [P_{Tx} P_{Ty} P_{Tz} 0\ 0\ 0]^T \tag{25}$$

provides for orthotropic thermal expansion.

It appears that the shrinkage is stress dependent. By considering such a stress dependence, it is possible to capture the *transient creep*, i.e. the phenomenon that the total time-dependent deformation when shrinkage and creep occur simultaneously is larger than the sum of the two, separate components would suggest. Bažant (1988) has shown that the viscosity dependence on humidity and thermal rate, which would explain the *transient creep*, is equivalent to a stress-induced shrinkage and thermal shrinkage. Therefore, a stress-dependent shrinkage is formulated here:

$$\begin{aligned} \dot{\boldsymbol{\varepsilon}}_s &= \alpha_s (\boldsymbol{P}_s + \boldsymbol{r}_s \sigma) \dot{h} \\ \dot{\boldsymbol{\varepsilon}}_T &= \alpha_T (\boldsymbol{P}_T + \boldsymbol{r}_T \sigma) \dot{T}. \end{aligned} \tag{26}$$

Provision is made for orthotropy by defining the stress-induced shrinkage and thermal expansion coefficient matrices as

$$\begin{aligned} \boldsymbol{r}_s &= diag[r_{sx} r_{sy} r_{sz} 0\ 0\ 0] \\ \boldsymbol{r}_T &= diag[r_{Tx} r_{Ty} r_{Tz} 0\ 0\ 0]. \end{aligned} \tag{27}$$

5 Case: Masonry drying shrinkage analysis

The model is demonstrated by the analysis of masonry free shrinkage and transient creep experiments reported in van der Pluijm and Wubs (1996), Figure 9.

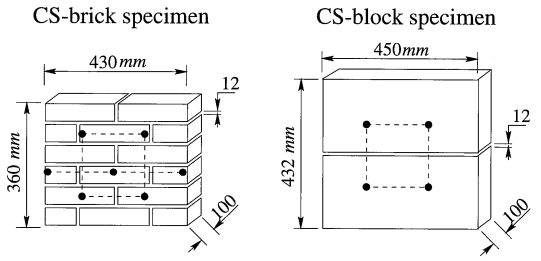

Fig. 9. Masonry shrinkage specimens investigated.

Due to the lack of characterisation data for masonry, the model parameters have been estimated from tests on similar materials, or derived from the global behaviour of wall parts. For one aspect, namely the apparent stress dependence of shrinkage, no experimental data exists for masonry. Therefore, an important goal of these analyses is to highlight the influence of particular mechanisms of creep and shrinkage to demonstrate the need for and aid in the design of customised experiments for the characterisation of creep and shrinkage of cementitious materials.

5.1 *Finite element model*

Full details of the analyses of both specimen types are given in van Zijl (2000). For brevity, only the specimen on the left in Figure 9 is reported here. It comprises calcium silicate bricks, joined with 12mm mortar joints. To investigate the moisture gradients and the resulting nonuniform shrinkage and eigen-stressing, three-dimensional discrete analyses have been performed, employing the interface model to capture delamination and shearing along the mortar-brick interfaces. The mortar and bricks have been modelled with 8-noded brick elements. For the hygral analysis special plane interface elements model the surface convection at the exposed face. The natural condition of zero flux has been modelled at the remaining edges, because the edges of each specimen were sealed in the experiments.

5.2 *Model parameters*

The diffusion coefficients d_θ are shown in Figure 10a. They can be derived from Nuclear Magnetic Resonance measurements of moisture profiles in one-dimensionally drying calcium silicate and mortar specimens respectively, by the solution of a one-dimensional diffusion equation with the moisture content as potential (Pel 1995). The hygroscopic relation $\theta(h)$ from which the absorption capacity c is obtained, is shown in Figure 10b.

The parameters needed to describe the mechanical behaviour are summarised in Tables 1 and 2. These parameters are based on the experimental studies (van der Pluijm and Vermeltfoort 1991, van der Pluijm 1992) of masonry joint failure.

The Maxwell creep model parameters have been obtained by least squares curve fitting of the measured creep data (van der Pluijm and Wubs 1996), Figure 11. With creep data lacking for the constituent materials separately, equal creep coefficients have been assumed for the bricks and mortar. Due to a lack of experimental data aging has not been considered.
The measurement of true shrinkage, i.e. the volume reduction of a material element at zero stress, is hampered by the slow drying process in cementitious materials which causes humidity gradients, eigenstresses and cracking. However, by the assumption of a constant shrinkage coefficient and by ignoring cracking and stress-induced shrinkage ($r_s = 0$ in eq. 26), the coefficients can be estimated from the "final" shrinkage strain (ε_s^∞) by $\alpha_s P_i = (\varepsilon_s^\infty) / (h_E - h_0)$. In this manner the parameters $\alpha_s = 0.0007$, $P_x = P_z = 1.0$, $P_y = 1.1$ have been obtained from the measured shrinkage data (van der Pluijm and Wubs 1996). Due to the absence of separate shrinkage data for the mortar and the bricks, the coefficients have been derived from the composite response and employed for each constituent.

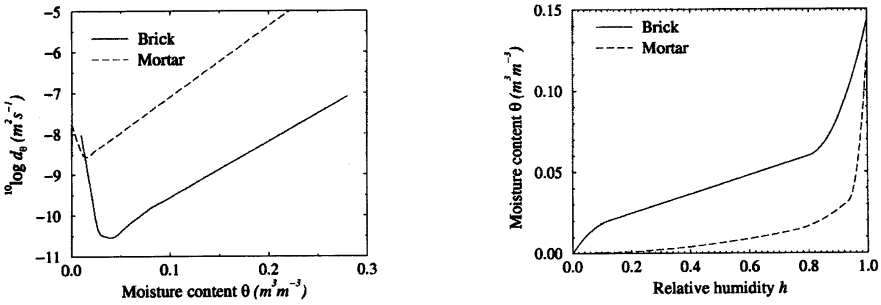

(a) *(b)*

Fig. 10. (a) Diffusion coefficient d_θ(Pel 1995) and (b) isothermal sorption curve.

Table 1: Mechanical material parameters.

Brick				Mortar		Interface					
E (MPa)	ν	f_t (MPa)	G_f^I ($\frac{N}{mm}$)	E (MPa)	ν	f_t (MPa)	G_f^I ($\frac{N}{mm}$)	c_o (MPa)	$\tan\phi_o$	$\tan\phi_r$	G_f^{II} ($\frac{N}{mm}$)
11500	0.2	2.0	0.06	3300	0.2	0.1	0.005	0.28	0.97	0.75	0.02-0.03σ

Elasticity: E = Young's modulus; ν = Poisson's ratio

Strength: f_t = tensile strength; c_o = original adhesion; ϕ_o = initial friction angle; ϕ_r = residual friction angle

Softening: G_f^I = tensile fracture energy; G_f^{II} = shear fracture energy; σ = normal stress (MPa)

Table 2: Dilatancy parameters employed.

$\tan\psi_o$	σ_u (MPa)	δ
0.67	-1.22	17

$$\Psi = \frac{\Delta u}{\Delta v} = \tan\psi_o \left(1 - \frac{\sigma}{\sigma_u}\right) e^{-\delta \Delta v}$$

Ψ = dilatancy coefficient; ψ_o = dilatancy angle at zero pressure and shear-slip

Δu = uplift normal to joint; σ_u = pressure inhibiting any uplift

Δv = shearing along joint; δ = gradient of surface smoothing with shear-slip

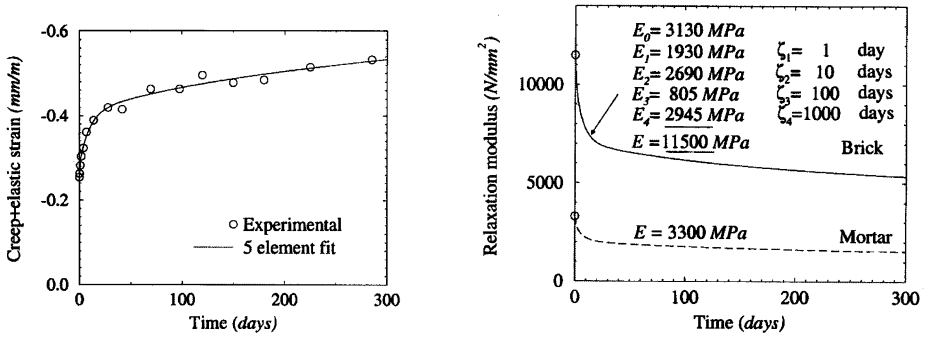

(a) (b)

Fig. 11: (a) Measured creep (van der Pluijm and Wubs 1996) and fitted five-element Dirichlet function. (b) Maxwell chain derived from (a), showing spring stiffnesses E and relaxation times ζ.

No experimental data is available from which the shrinkage stress-dependence coefficients r_s, eq. (26) can be estimated. They have been set equal to zero for the initial analyses. Subsequently the maximum and minimum values reported for concrete ($0.2/f_t \le r_i \le 0.8/f_t$) (Bažant and Chern 1985) have been employed to demonstrate their significance.

5.3 *Boundary conditions and initial values*

The experiments were conducted at a controlled climate of 20°C and h_E =0.5. For a zero air flow velocity a surface convection transfer coefficient β =5 mm/day is appropriate.

The calcium silicate elements were pre-wetted to a moisture content between 6% and 8% by mass, according to standard building procedures for this material. With the assumption of an initially uniform pore humidity and a hydraulically perfect interface between the mortar and brick, h_0=0.96 has been calculated from the hygroscopic curve.

5.4 *Results*

Figures 12a-b show the maximum principal eigen-stresses accompanying the hygral gradients for the case of free shrinkage. In the early stages high tensile stresses occur at the surface, causing initiation of debonding. The brick strength (2 MPa) is also slightly exceeded in the brick faces, so that drying cracks could develop there, but this fact is ignored in the modelling strategy. As time passes the peak stresses reduce along with the hygral gradients until a virtually (eigen-)stress-free state after 100 days. Note that the deformations have been scaled up by a factor of 500. The maximum crack width is in the order of 7 μm, reached after ten days. A closer look in the interface zone is required to confirm the predicted delamination along all the brick-mortar interfaces. Such small cracks can only be detected with special experimental techniques, which were not applied in these experiments. However, the predicted delamination along the interfaces is in line with the observation reported by van der Pluijm (1999) that only approximately the central half to two thirds of a typical masonry joint surface remains bonded after drying shrinkage.

Figure 12c shows that reasonable agreement is obtained between the measured and numerical average strains in the gauge length in the x direction, as well as in the y direction. If the debonding at the interfaces is not included in the model, a significantly larger shrinkage, the dashed line in Figure 12c, is obtained in the y direction, where 3 delaminating interfaces are included in the gauge length. As the shrinkage parameters have been estimated ignoring the influence of cracking, the uncracked numerical response represents the experimental response well.

The response to the added 2.5 MPa compressive creep load is shown in Figure 13a, for various choices of the coefficient of stress-induced shrinkage $r_s = r_{sx} = r_{sy} = r_{sz}$. As the Maxwell chain has been fitted to the experimental creep data with the assumption that $r_s = 0$, this case agrees with the measured response. Within the range of this coefficient observed for concrete (Bažant and Chern 1985) ($0.2/f_t \leq r_s \leq 0.8/f_t$) a significant influence is seen, Figure 13a. The total compressive strain is increased by up to 30%, which means that, if such a dependence does exist, the experimentally measured basic creep is overestimated, Figure 13b, because it contains the stress-induced shrinkage strain component not reflected by the free shrinkage. Only by testing similar, but non-drying creep specimens the error can be quantified (van Zijl 1999).

An additional source of error is also unveiled in Figure 13b. Cracking reduces the material (stress-free) shrinkage in the free drying specimen, but does not occur in the creep specimen, the tensile stresses being offset sufficiently by the creep load.

6 Conclusions

A numerical model has been proposed for the analysis of the time-dependent behaviour of cementitious materials, like concrete and masonry. The time dependence is captured by combining linear visco-elasticity with smeared or discrete cracking models and considering the FPZ viscosity.

The capability of the model to capture the time-dependent crack propagation has been validated by the analysis of creep failure experiments. The correct rate-dependent strength as well as the correct time scale are introduced by the rate terms. Thereby, the expected life of a structure can be predicted. This enables concrete and masonry structures to be designed for a particular duration.

The numerical model has a simple framework, which enables the incorporation of hygral and thermal shrinkage. The shrinkage evolution must be computed initially. A nonlinear diffusion equation and its numerical solution in terms of the pore relative humidity has been proposed for this purpose. From the pore humidity solution the hygral shrinkage can be calculated, which enters the mechanical model. The thermal shrinkage can be calculated in an analogous way by solving a heat conduction equation. However, for simultaneous hygral and thermal variation, a set of coupled differential equations have to be solved, which has not been attempted in this study. This one-way coupled diffusion and mechanical analysis has been demonstrated in the analysis of masonry creep and shrinkage experiments. Reasonable agreement with the global, observed response has been obtained.

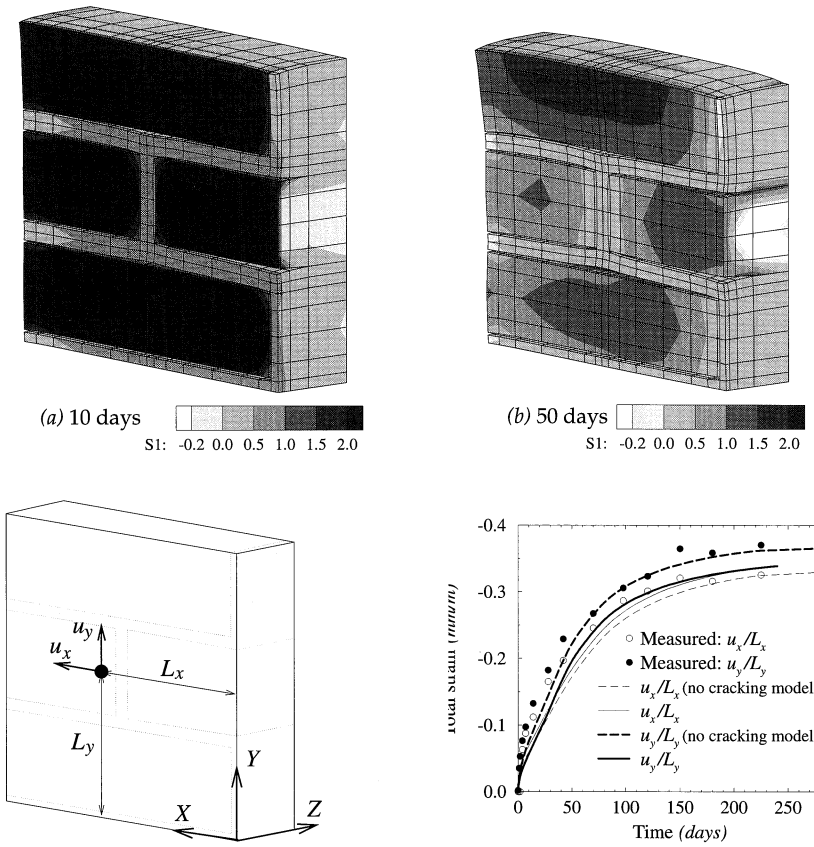

Fig. 12: (a-b) Contours of maximum principal stress (MPa) and (c) total strain in the gauge length in free drying CS-brick specimen.

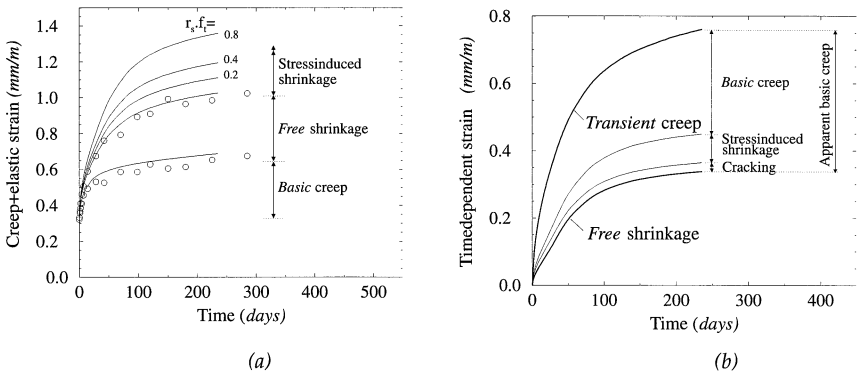

Fig. 13: (a) Transient creep response. (b) Illustration of error in basic creep estimation.

Acknowledgements

The authors gratefully acknowledge the financial support by the Netherlands Technology Foundation (STW) under the grant DCT 44.3406. The models were implemented in pilot versions of DIANA.

References

BAŽANT, Z.P. (1988). Material models for structural creep analysis. *Mathematical Modelling of Creep and Shrinkage of Concrete* (ed. Z.P. Bažant), John Wiley and Sons, Ch. 2, 99-215.

BAŽANT, Z.P. and CHERN, J.C. *(1985).* Concrete creep at variable humidity. *Mat. and Struct.*, **18**(103), 1-20.

BAŽANT, Z.P. and NAJJAR, L.J. (1971). Drying of concrete as a nonlinear diffusion problem. *Cement and Concrete Research*, **1**(**5**), 461-73.

BECKER, E.B., CAREY, G.F. and ODEN, J.T. (1981). *Finite Elements: An introduction.* Prentice-Hall, Englewood Cliffs, New Jersey, USA.

BINDA, L., Gatti, G., MANGANO, G., POGGI, C. and SACCHI-LANDRIANI, G. (1992). The collapse of the Civic Tower of Pavia. *Masonry International* **1**, 27-3 6.

DE BORST, R. (1986). Smeared cracking, plasticity, creep and thermal loading - a unified approach. *Computer Methods in Applied Mechanics and Engineering*, **62**, 89-110.

DE BORST, R., VAN DEN BOOGAARD, A.H., SLUYS, L.J. and VAN DEN BOGERT, P.A.J. (1993). Computational issues in time-dependent deformation and fracture in concrete. *Creep and Shrinkage of Concrete* (eds. Z.P. Bažant and I. Carol). E.&FN.Spon, London, 309-325.

FEENSTRA, P.H. (1993). *Computational aspects of biaxial stress in plain and reinforced concrete.* Dissertation, Delft Univ. of Techn., Delft, The Netherlands.

L'HERMITE, R. and MAMILLAN, M. (1968). Retrait et fluage des bétons (in French), *Annales A TB TP*, **21**(249), 1319-37.

LOURENÇO, P.B. (1996). *Computational strategies for masonry structures.* Dissertation, Delft Univ. of Techn., Delft, The Netherlands.

PEL, L. (1995). *Moisture transport in porous building materials.* Dissertation, Eindhoven Univ. of Techn., Eindhoven, The Netherlands.

PHILIP, J.R. and DE VRIES, D.A. (1957). Moisture movement in porous materials under temperature gradients, *Trans. Am. Geophys. Un.*, **38**(2), 222-32.

ROTS, J.G. (1997). *Structural masonry; an experimental/numerical basis for practical design rules.* Balkema: Rotterdam, 1997.

SLUYS, L.J. (1992). *Wave propagation, localisation and dispersion in softening solids.* Dissertation, Delft University of Technology: Delft, The Netherlands.

TAMMES, E. and VOS, B.H. (1984). *Heat and moisture transport in building structures* (in Dutch). Kluwer, Deventer-Antwerpen.

VAN DER PLUIJM, R. (1992). *Deformation controlled shear tests on masonry* (in Dutch). Report BI-92- 104, TNO Building and Construction, Delft, The Netherlands.

VAN DER PLUIJM, R. and VERMELTFOORT, A.Th. (1991). *Deformation controlled tension and compression tests on units, mortar and masonry* (in Dutch). Report B-91-0561, TNO Building and Construction, Delft, The Netherlands.

VAN DER PLUIJM, R. and WUBS, A.J. (1996). *The time dependent deformational behaviour of masonry* (in Dutch). Report 96-CON-R0901-02, TNO Building and Construction, Delft, The Netherlands.

VAN ZIJL, G.P.A.G. (1999). *A numerical formulation for moisture migration in masonry.* Series 11 Eng. Mech. 02, Delft Univ. Press, Delft, The Netherlands.

VAN ZIJL, G.P.A.G. (2000). *Computational Modelling of Masonry Creep and Shrinkage.* Dissertation: Delft University of Technology, Delft, The Netherlands.

WITTMANN, F.H. (1977). Grundlagen eines Modells zur Beschreibung charakteristischer Eigenschaften des Betons (in German), *Schriftenreihe DeutscherAusschuss für Stahlbeton,* Heft 290, Berlin, 43- 101.

WU, Z.S. and BAŽANT, Z.P (1993). Finite element modelling of rate effect in concrete fracture with influence of creep. *Creep and Shrinkage of Concrete* (eds. Z.P. Bažant and I. Carol). E.&FN.Spon, London, 427-432.

ZHOU, F.P. (1992). *Time-dependent crack growth and fracture in concrete.* Dissertation, Lund University, Lund, Sweden.